Optics Letters

Low-dimensional nano-patterned surface fabricated by direct-write UV-chemically induced geometric inscription technique

T. Allsop,[1,4,*] R. Neal,[2] V. Kundrat,[1] C. Wang,[1] C. Mou,[3] P. Culverhouse,[2] J. D. Ania-Castanon,[4] K. Kalli,[5] and D. J. Webb[1]

[1]Aston Institute of Photonic Technologies, Aston University, Aston Triangle, Birmingham B47ET, UK
[2]Faculty of Science and Technology, School of Computing, Electronics and Mathematics, University of Plymouth, Plymouth PL4 8AA, UK
[3]Key Laboratory of Special Fiber Optics and Optical Access Network, Shanghai University, Shanghai 200072, China
[4]Non-linear Dynamics and Fiber Optics, Instituto de Óptica "Daza de Valdés" (IO-CSIC), Calle de Serrano, 121, 28006 Madrid, Spain
[5]Department of Electrical Engineering, Computer Engineering and Informatics, Cyprus University of Technology, Lemessos 3036, Cyprus
*Corresponding author: t.d.p.allsop@aston.ac.uk

Received 24 October 2018; revised 27 November 2018; accepted 27 November 2018; posted 30 November 2018 (Doc. ID 349130); published 2 January 2019

We investigate a nano-patterning process which creates reproducible periodic surface topological features that range in size from ~100 μm to ~20 μm. Specifically, we have fabricated multi-layered thin films consisting of germanium/silicon strata on a planar substrate, with each layer having nanometers thickness. The material processing exploits focused 244 nm ultra-violet laser light and an opto-mechanical setup typically applied to the inscription of fiber gratings, and is based upon the well-known material compaction interaction of ultra-violet light with germanium oxides. We show this process can be extended to create arrays of metal nano-antennas by adding a metal overlay to the thin film. This results in arrays with dimensions that span nanometer- to centimeter-length scales. Also, each nano-antenna consists of "nano-blocks." Experimental data are presented that show the UV irradiance dosage used to create these metal nanostructures on D-shaped optical fibers has a direct relationship to their transmission spectral characteristics as plasmonic devices.

https://doi.org/10.1364/OL.44.000195

The creation of nanometer-scale surface features is often realized by means of photolithography, and this has proven to be important to various areas of technology and science, but in particular to electronics/printed circuits [1,2]. Advances have been realized with the advent of UV-nanoimprint lithography, (UVNL) [3,4], extreme ultraviolet (EUV) lithography [5], and laser interference lithography (LIL) [6]. The drive for the development of the UVNL, EUV, and LIL is the production of cost-effective lithographic patterning that offers high accuracy for integrated circuitry, along with the possibility of new nano-scale devices for optical devices [6]. Of particular relevance to our work is the application of photolithography in the fabrication of surface plasmon (SP) sensors, with a focus on biosensors [4,7,8]. We note that many differing surface topologies can be used to generate SPs, e.g., holes and table/disc shapes of varying sizes [9,10].

A common factor in all of the fabrication techniques and the resultant sensors is their duration and complexity of the required procedures. This can be seen in UVNL, EUV, and LIL, which use photoresist materials and require multiple-stage processing, such as mechanical imprinting, the spinning of a photoresist, UV exposure, and etching techniques, along with wet chemistry procedures [3–10]. The fabrication procedure that we report here is based upon the spatial structural changes of Ge brought about by its interaction with UV laser light, a physical phenomenon that is typically used to produce grating devices in optical fibers [11] and is investigated using planar samples [12]. It is based upon photo bleaching [11]. This process consists of two physical mechanisms, namely, the change in electron density of specific Ge═O/Ge O bonds, effectively a redox reaction, thus changing the permittivity and structural change in the material; and the spatial compaction of the material itself. This second mechanism is used to create the spatial geometric surface features reported here.

This process does not use etching, wet chemistry, or photoresists in the fabrication process, thus reducing fabrication complexity. We use a focused 244 nm UV laser working in conjunction with a phase mask in the fabrication of uniform corrugations on a Ge-coated surface at nanometer scale, along with the production of concentric circles on a micrometer scale. Furthermore, the Ge layer has additional over-layers consisting of silicon dioxide and a metal (Ag, Au, or Pt); using these coatings with the technique described here produces arrays of nanowires supported on the silicon dioxide substrate (or polished/D-shaped optical fibers). The size of the surface topological features ranges from ~100 μm to ~10 μm, along with

the creation of sub-micrometer (500 nm) periodic structures that are repeatable, of a total length in excess of 2 cm. These nano-antenna arrays can be used as parts on an optical sensing platform for biological and chemical sensors. The interaction of the Ge layer and the 244 nm UV light was investigated, where a thin film coating of Ge of a thickness of 48 nm was deposited upon a series of BK7 glass substrates of thickness 150 μm [13]. All the thin films were deposited using an RF sputtering machine (Nordico 6 inch RF/DC three-target excitation machine). The Ge-coated planar substrates were mounted and spatially aligned for exposure to various intensities of laser light at 244 nm, in an opto-mechanical arrangement similar to that used for the UV inscription of optical fiber gratings [11], with the following three configurations: (1) single axis with the laser beam focused along the line of travel of an air-bearing stage for controlled motion, using a plano-convex lens focal length of 80 mm, followed by a phase mask (period of 1.018 μm); (2) laser beam focused on two axes parallel and perpendicular to line of travel of the air-bearing stage (using two plano-convex lenses, both having focal lengths of 80 mm); and (3) a combination of (1) and (2) (Fig. 1).

A series of experiments were conducted on a number of Ge-coated surfaces using various laser inscription powers, from 100 mW to 180 mW of 244 nm UV laser light (Argon Ion laser, Sabre Fred Coherent Inc) and using a constant scan velocity of 0.1 m/s for the three focusing arrangements, shown in Fig. 1(b). Varying the laser's irradiance pattern on the surface of the various samples creates surface features and topologies that resemble the spatial intensity variation of the UV laser light. Using configuration 1 (phase mask and single lens combination) produced two main surface features, a fine nanoscale corrugation with an amplitude related to the irradiance on the sample and a secondary background feature with greater physical height measured using an atomic force microscope (AFM, Park Systems XE-200) [Fig. 2]. Figure 2(a) shows the overall diffraction pattern produced by the phase mask with predominant periods ~18 μm (the variation in maximum height of the surface features from left to right is due to error in the alignment of the sample to the laser, resulting from human involvement/error in the present alignment procedure that dominants the variations in the final corrugation physical characteristics). Figure 2(b) shows the interference pattern produced from the overlapping fringes, with the predominant periods in the range of 0.5–1.1 μm. The relationship between the surface feature size and irradiance depends upon the optical setup, e.g., using setup (2) saturation occurring at the lower energies' regime,

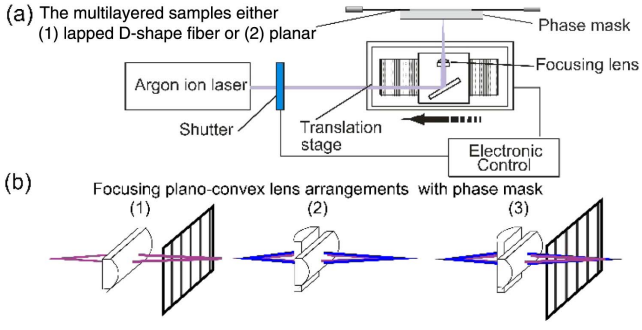

Fig. 1. (a) Schematic of opto-mechanical apparatus for the creation of the surface structures on planar and optical fiber substrates. (b) Spatial focusing setup of the plano-convex lenses and phase mask.

creating features with heights of 0.6 μm. The fine surface structure period varied with irradiance for the given phase mask. These results obtained from the samples are normalized and summarized in Figs. 3(a)–3(d), whereas the inspections of fine structure results are shown in Figs. 3(a) and 3(c). Observations in these results indicate that increasing the irradiance increases the number of smaller periods and has a saturation effect on surface corrugation amplitude, reaching 7–10 nm [Fig. 3(c)].

The degree of misalignment of the sample under processing to the focal plane of the UV light dictates the size background features created by the near-field Fresnel diffraction compared to the features created in the far-field Fraunhofer diffraction interference pattern (a classic irradiance pattern; Fresnel diffraction of a rectangular aperture of width exceeding the wavelength of flight). This saturation effect is understandable, as there is only a limited amount of Ge within the coating. Also, as the irradiance rises, the average absorption of UV light per unit area increases over an average fringe oscillation. Therefore, the maximum amplitude in the background spatial perturbation decreases with increasing number of scans, effectively a controlled "washing out" of the pattern [Fig. 3(d)].

Following this initial set of experiments, additional layers were deposited upon the Ge of silicon dioxide (48 nm thickness) followed by metal films of Au, Ag (both with 32 nm thickness), or Pt (36 nm thickness); these thicknesses where chosen from the modeling undertaken in Ref. [14]. AFM scans for an Au-coated sample are shown in Fig. 4, showing corrugated regions and an unexposed region of the multi-layered coating (no surface corrugation) [Fig. 4(a)]. The resultant height of the corrugation varied with the overlay metal; typically, Ag yielded ~110 nm, Au a height of ~70 nm, and Pt reached ~40 nm. The two reasons for this height variation with metals are: first, we must consider skin depth effects for the metals

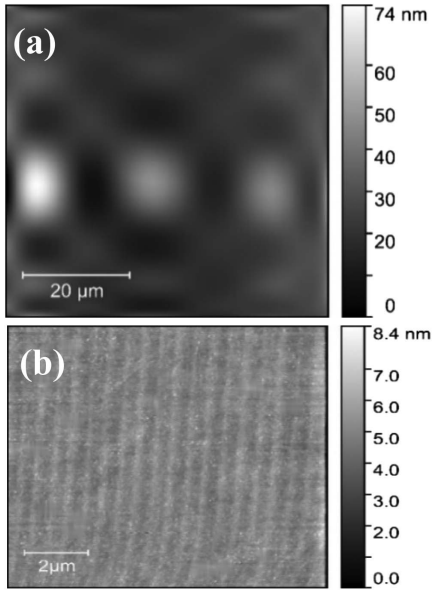

Fig. 2. Variation of the surface topology for a Ge-coating (48 nm depth) on a planar substrate, following 244 nm UV laser processing (power: 180 mW, scan velocity: 0.1 mm/s) through a phase mask (period: 1.018 μm). (a) AFM map of the diffraction pattern resulting from laser irradiation, with the sample placed 40 μm beyond the laser focal point and the Fraunhofer diffraction. (b) AFM map of the finer interference pattern produced by the diffracted beams.

($d_s = \lambda/4\pi\kappa$, where λ is wavelength and κ is attenuation index [14]), and the skin depth for Ag at 244 nm is ~35 nm compared to ~13 nm for Au and ~10 nm for Pt; therefore, greater UV irradiance reaches the Ge layer in the case of Ag, inducing a greater reaction with Ge and higher compaction, and yielding the highest amplitude of corrugation. Second is the melting point for silver; 961.8°C is the lowest of the metals used, whereas it has the greatest thermal conductivity, 429 $Wm^{-1}\,k^{-1}$ [13], which helps to transfer the generated thermal energy to the Ge region, making the material more malleable. Of course, it is the inclusion of the metal overlay in the sputtering procedure that creates the array of nano-antennas during UV-laser exposure.

Also, the finer resolution AFM scan of the UV-processed regions revealed structure within a nano-antenna [Fig. 4(b)]. Fast Fourier transform analysis (FFT) was performed on the single profile of individual nano-antennas and across-sections between nano-antennas [Fig. 4(c) and 4(d), respectively]. The FFT revealed prime periods of 0.54 μm and 1.02 μm, which is expected due to a phase-mask period of ~1 μm [Figs. 4(c) and 4(d)]. Second, the fundamental period within an individual antenna is 0.29 μm. This can be explained in that the phase mask generates a fringe pattern in three dimensions—a series of phase planes where the irradiance intensity varies across each of the planes perpendicular to the sample surface. However, generally these phase planes are not ideally parallel to the surface plane of the sample being processed. In practice, this nominal angle between the sample surface and the phase plane, when combined with the pattern focused upon the planar

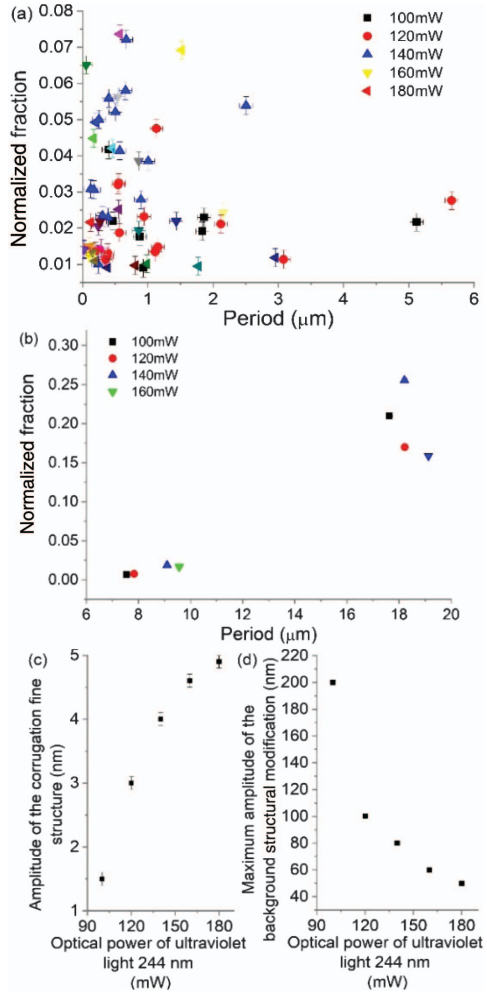

Fig. 3. Spatial features of the UV-light-irradiated Ge-coated sample (48 nm thickness) on planar samples. (a) Periods of the fine corrugation produced from the UV light interference pattern. (b) Periods of the background spatial perturbation created by the diffraction pattern. (c) Amplitude of the fine corrugations. (d) Maximum variation height of the background spatial perturbation.

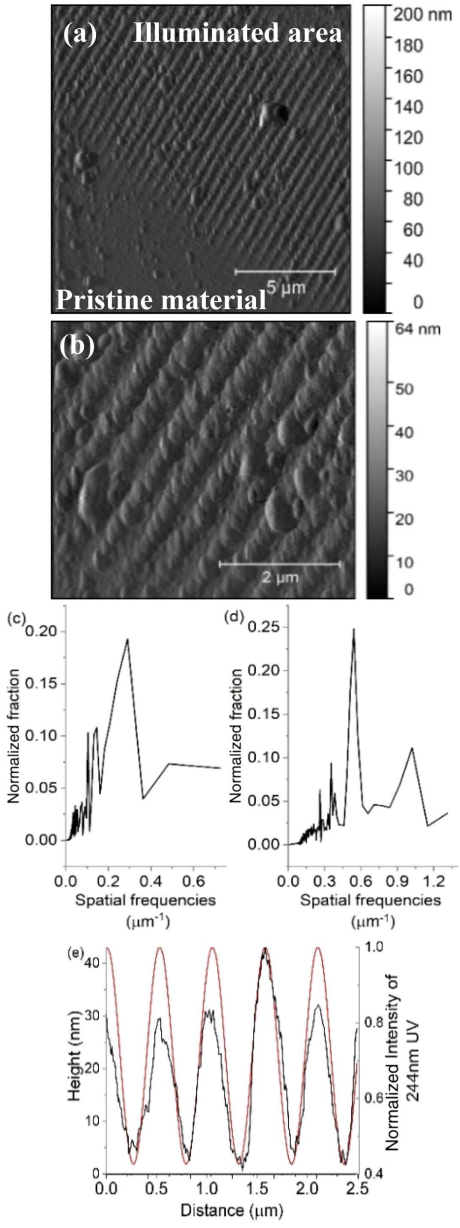

Fig. 4. Surface corrugation for a multi-layered coating (48 nm Ge, 48 nm SiO_2, and 32 nm Au) on a planar substrate. (a) AFM scan showing regions of pristine coating with no exposure and exposed regions with nano-structuring. (b) AFM scan showing the secondary detail of the topology associated with each of the individual nano-antennas. (c), (d) Variations of the spatial frequencies along a nano-antenna and across the nano-antennas, respectively. (e) Typical cross-section profile of surface topology for an Au metal overlay of thickness 32 nm along with the normalized irradiance pattern generated with the 1.018 μm phase mask illumined with 244 nm.

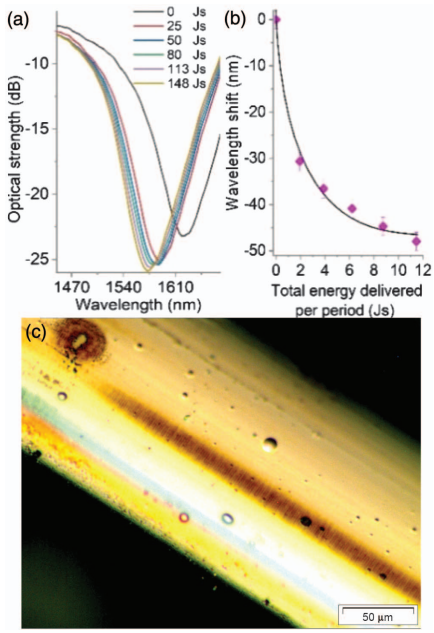

Fig. 5. (a) Spectral behavior of a D-shaped optical fiber device with a Pt metal layer (36 nm) as a function of the UV-laser dosage. (a) Transmission spectra, (b) wavelength shift, and (c) microscopic image of a section of the nanowire array created by the technique reported.

sample, results in a "bead-like" pattern; thus, as the scalar dot product between the sample's surface and the phase plane decreases, the more prominent this feature becomes. The size/repeatability of shape is limited by human error in the fiber alignment (position and orientation) to the phase mask during fabrication [Fig. 4(b)].

As discussed, these structures can create SPs when illuminated with polarized light and are the subject of research at the moment by the authors [13–15]. In order to examine the generation of SPs, the aforementioned laser structuring is performed on multi-layered samples deposited on polished or D-shaped optical fibers, and the transmission spectrum of the optical fiber is monitored, from which changes in the laser-structured region can be distinguished. During the fabrication procedure, using multi-exposures of UV-laser irradiance, the SP resonance (SPR) monitored in the fiber transmission spectrum, using the arrangement used in Ref. [12], shifts to a different wavelength [Fig. 5(a)]. The wavelength shift can be either red or blue, depending upon the dispersion characteristics of the SP and the material being used. This spectral behavior is anticipated due to the fact that the SPR depends on the size and shape of the nano-antennas supporting the SP [9,10,16], and Fig. 3 shows that increasing the UV-laser dosage to Ge layer increases the amplitude of the corrugations [Fig. 3(c)] along with varying the period of the corrugations. The Ge layer is spatially compact due to UV irradiance and with the additional deposited layers (i.e., the metal overlay) produces regions of metal on the apex of the corrugations: nanowires [13]. A typical cross-section profile of surface topology is shown in Fig. 4(e), along with the calculated irradiance spatial distribution created by the phase mask, which shows agreement to the location of the maximum these calculated results have assumed simple Fraunhofer diffraction convolution with a beam spot size 0.3 mm and distance of 3 µm from the phase mask to the sample. Typical standard deviations are 11% from the average height and 9% from the average width of the corrugation. Also, for completeness, the typical UV fabrication time to create a 2 cm length is 5–10 min; Fig. 5(c) shows a section of a fabricated array of nanowires, of length 400 µm. Comparing these results to those in Ref. [12], there is greater flexibility/complexity over a larger surface area. Inspecting the AFM map in Ref. [14] shows more variations in the periods in the array compared to the AFM map of the arrays reported here, demonstrating more reproducibility and repeatability, leading to superior plasmonic devices.

In conclusion, we have presented a simple procedure to flexibly create complex, repeatable surface structures from micrometer- to centimeter-length scales using a novel and relatively inexpensive fabrication method. We have shown that this fabrication method has the potential to create low-dimensional material nano-structuring for applications such as plasmonics.

Funding. Engineering and Physical Sciences Research Council (EPSRC) (EP/J010391, EP/J010413); H2020 Marie Skłodowska-Curie Actions (MSCA) COFUND Action MULTIPLY (713694).

Acknowledgment. The authors' contributions are: T. A. developed the concept; T. A. modeled, designed, and performed experiments and analyzed the experimental data; T. A., C. M., and R. N. fabricated and UV processed the test samples; and V. K., T. A., and K. K. characterized materials and performed experiments. The Letter was written by all authors.

REFERENCES

1. D. A. Campo and C. Greiner, J. Micromech. Microeng. **17**, R81 (2007).
2. S. V. Sreenivasan, Microsyst. Nanoeng. **3**, 17075 (2017).
3. S. Matsui, in *16th International Conference on Nanotechnology (IEEE-NANO)* (2016), pp. 706–709.
4. A. Cattoni, P. Ghenuche, A.-M. Haghiri-Gosnet, D. Decanini, J. Chen, J.-L. Pelouard, and S. Collin, Nano Lett. **11**, 3557 (2011).
5. B. Päivänranta, A. Langner, E. Kirk, C. David, and Y. Ekinci, Nanotechnology **22**, 375302 (2011).
6. J.-H. Seo, J. H. Park, Z. Ma, J. Choi, and B.-K. Ju, J. Nanosci. Nanotechnol. **14**, 1521 (2014).
7. J. Anker, P. Hall, O. Lyandres, N. C. Shah, J. Zhao, and R. P. Van Duyne, Nat. Mater. **7**, 442 (2008).
8. S.-W. Lee, K.-S. Lee, J. Ahn, J.-J. Lee, M. G. Kim, and Y.-B. Shin, ACS Nano **5**, 897 (2011).
9. D. B. Shao and S. C. Chen, Nano Lett. **6**, 2279 (2006).
10. W. Srituravanich, N. Fang, Q. Luo, and X. Zhang, Nano Lett. **4**, 1085 (2004).
11. K. O. Hill, B. Malo, F. Bilodeau, D. C. Johnson, and J. Albert, Appl. Phys. Lett. **62**, 1035 (1993).
12. F. J. Young, J. E. Sipe, and H. M. Van Driel, Phys. Rev. B **30**, 2001 (1984).
13. T. Allsop, R. Neal, C. Mou, K. Kalli, S. Saied, S. Rehman, D. J. Webb, P. F. Culverhouse, J. L. Sullivan, and I. Bennion, IEEE J. Quantum Electron. **48**, 394 (2012).
14. T. Allsop, R. Neal, C. Mou, P. Brown, S. Saied, S. Rehman, K. Kalli, D. J. Webb, J. Sullivan, D. Mapps, and I. Bennion, Appl. Opt. **48**, 276 (2009).
15. T. Allsop, R. Arif, R. Neal, K. Kalli, V. Kundrát, A. Rozhin, P. Culverhouse, and D. J. Webb, Light: Sci. Appl. **5**, e16036 (2016).
16. K. L. Kelly, E. Coronado, L. L. Zhao, and G. C. Schatz, J. Phys. Chem. B **107**, 668 (2003).